

LIMITS ON THE LORENTZ INVARIANCE VIOLATION FROM UHECR ASTROPHYSICS.

RODRIGO GUEDES LANG,¹ HUMBERTO MARTÍNEZ-HUERTA,^{1,2} AND VITOR DE SOUZA¹

¹*Instituto de Física de São Carlos, Universidade de São Paulo, Av. Trabalhador São-carlense 400, São Carlos, Brasil.*

²*Departamento de Física, Centro de Investigación y de Estudios Avanzados del I.P.N., Apartado Postal 14-740, 07000, Ciudad de México, México.*

(Received December 3, 2024; Revised; Accepted)

Submitted to ApJ

ABSTRACT

In this paper, Lorentz Invariance Violation (LIV) is introduced in the calculations of photon propagation in the Universe. LIV is considered in the photon sector and the mean free path of the $\gamma\gamma \rightarrow e^+e^-$ interaction is calculated. The corresponding photon horizon including LIV effects is used to predict major changes in the propagation of photons with energy above 10^{18} eV. The flux of GZK photons on Earth considering LIV is calculated for several source models of ultra-high energy cosmic ray (UHECR). The predicted flux of GZK gamma-rays is compared to the upper limits on the photon flux obtained by the Pierre Auger Observatory in order to impose upper limits on the LIV coefficients of order $n = 0, 1$ and 2 . The limits on the LIV coefficients derived here are several orders of magnitude more restrictive than those derived for TeV photons. An important update of the limits on LIV using GZK photons is also presented using new astrophysical scenarios and data.

Keywords: cosmic rays - Lorentz invariance violation

1. INTRODUCTION

Astroparticle physics has recently reached the status of precision science due to: a) the construction of new observatories operating innovative technologies, b) the detection of large numbers of events and sources and c) the development of clever theoretical interpretations of the data. Two observational windows have produced very important results in the last decade. The ultra-high energy cosmic rays ($E > \text{EeV}$) studied by the Pierre Auger and the Telescope Array Observatories ([The Pierre Auger Collaboration \(2015\)](#); [Tinyakov \(2014\)](#)) improved our knowledge of the most extreme phenomena known in Nature. The GeV-TeV gamma-ray experiments FERMI/LAT ([Atwood et al. \(2009\)](#)), H.E.S.S. ([The H.E.S.S. Collaboration \(2006\)](#)), MAGIC ([The MAGIC Collaboration \(2016\)](#)) and VERITAS ([J. Holder for the VERITAS Collaboration \(2011\)](#)) gave a new perspective on gamma-ray production and propagation in the Universe. The operation of the current instruments and the construction of future ones ([The CTA Consortium \(2011\)](#); [Haungs et al. \(2015\)](#)) guarantee the production of even more precise information in the decades to come.

Lorentz Invariance (LI) is one of the pillars of modern physics and it has been tested in several experimental approaches ([Mattingly \(2005\)](#)). Astroparticle physics has been proposed as an appropriate test environment for possible Lorentz Invariance Violation (LIV) given the large energy of the particles, the large propagation distances, the accumulation of small interaction effects and recently the precision of the measurements ([Liberati & Maccione \(2009\)](#); [Stecker & Scully \(2005, 2009\)](#); [Amelino-Camelia et al. \(1998\)](#); [Jacobson et al. \(2003\)](#); [Galaverni & Sigl \(2008a,b\)](#)).

Gamma-ray propagation in the intergalactic photon background was studied previously in detail by [De Angelis et al. \(2013\)](#). In the present work, LIV is allowed in the interaction of high energy photons with the background and its consequences are studied. The LIV framework is explained in section 2. A similar approach to that proposed by [Galaverni & Sigl \(2008a\)](#) is followed here. Only the $\gamma\gamma \rightarrow e^+e^-$ interaction is considered to violate Lorentz Invariance. The broken symmetry leads to a change of the energy threshold of the interaction. An independent solution of the allowed kinematic of the interaction under a given LIV model is presented and discussed.

The effect of the change in the energy threshold modifies the mean free path of the interaction and therefore the survival probability of a photon propagating in the background depends on the LIV coefficients. This dependence is calculated in section 3 in which the mean free path and the survival probability are shown for several LIV coefficients and expansion orders of the energy dispersion relation.

Finally, the mean free path of the $\gamma\gamma$ interaction considering LIV is implemented in a Monte Carlo propagation code. The effect of LIV in the flux of ultra-high energy photons arriving on Earth due to the GZK effect ([Greisen \(1966\)](#); [Zatsepin & Kuz'min \(1966\)](#)) is calculated considering several models for the sources of cosmic rays. The astrophysical model used to describe the primary cosmic ray flux has a very large influence on the flux of GZK photons and therefore on the LIV limits imposed. Section 4 quantifies the influence of the astrophysical models concerning mass composition, energy spectra shape and source distribution. These dependencies have been largely neglected in previous studies and it is shown here that they influence the GZK photon flux by as much as four orders of magnitude.

The propagated GZK photon flux for each model is compared to recent upper limits on the flux of photons obtained by the Pierre Auger Observatory. For some astrophysical models, the Auger data is used to set restrictive limits on the LIV coefficients.

2. DESCRIPTION OF THE LIV MODEL

One of the most commonly used mechanisms to introduce LIV in particle physics phenomenology is based on the polynomial correction in the dispersion relation of a free propagating particle, mainly motivated by an extra term in the Lagrangian density that explicitly breaks Lorentz symmetry, see for instance references [Amelino-Camelia et al. \(1998\)](#); [Coleman & Glashow \(1999\)](#); [Jacobson et al. \(2003\)](#); [Galaverni & Sigl \(2008a,b\)](#); [Maccione & Liberati \(2008\)](#); [Liberati & Maccione \(2011\)](#). In these models, the corrected expression for the dispersion relation is given by the following equation:

$$E_a^2 - p_a^2 = m_a^2 + \delta_{a,n} E_a^{n+2}, \quad (1)$$

where a denotes the particle with mass m_a and four-momenta (E_a, p_a) . For simplicity, natural units are used in this work. The LIV coefficient, $\delta_{a,n}$, parametrizes the particle dependent LIV correction, where n expresses the correction order, which can be derived from the series expansion or from a particular model for such order, see for instance the case of $n = 0$ ([Klinkhamer & Schreck \(2008\)](#)), $n = 1$ ([Myers & Pospelov \(2003\)](#)) or for a generic n ([Vasileiou et al. \(2013\)](#)). The LIV parameter of order n , δ_n , is frequently considered to be inversely proportional to some LIV energy scale $E_{LIV}^{(n)}$. Different techniques have been implemented in the search of LIV signatures in astroparticle physics and some of them have been used to derive strong constraints to the LIV energy scale ([Amelino-Camelia et al. \(1998\)](#); [Maccione & Liberati](#)

(2008); The H.E.S.S. Collaboration (2011); Vasileiou et al. (2013); Benjamin Zitzer for the VERITAS Collaboration (2014)).

Equation 1 leads to unconventional solutions of the energy threshold in particle production processes of the type $AB \rightarrow CD$. In this paper, the $\gamma\gamma_{CB} \rightarrow e^+e^-$ interaction is considered. From now on, the symbol γ refers to a high energy gamma ray with energy $E_\gamma = [10^9, 10^{22}]$ eV that propagates in the Universe and interacts with the cosmic background (CB) photons, γ_{CB} , with energy $\epsilon = [10^{-11}, 10]$ eV.

Considering LIV in the photon sector, the specific dispersion relations can be written:

$$\begin{aligned} E_\gamma^2 - p_\gamma^2 &= \delta_{\gamma,n} E_\gamma^{n+2}, \\ \epsilon^2 - p_{\gamma_{CB}}^2 &= \delta_{\gamma,n} \epsilon^{n+2}, \end{aligned} \quad (2)$$

where $\delta_{\gamma,n}$ is the n -order LIV coefficient in the photon sector and therefore taken to be the same in both dispersion relations. The standard LI dispersion relation for the electron-positron pair follows: $E_{e^\pm}^2 - p_{e^\pm}^2 = m_e^2$.

Taking into account the inelasticity (K) of the process ($E_{e^-} = KE_\gamma$) and imposing energy-momentum conservation in the interaction, the following expression for a head-on collision with collinear final momenta can be written to leading order in $\delta_{\gamma,n}$

$$4\epsilon E_\gamma - m_e^2 \left(\frac{1}{K(1-K)} - \frac{m_e^2}{2K(1-K)(E_\gamma + \epsilon)^2} \right) = -\delta_{\gamma,n} E_\gamma^{n+2} \left[1 + \frac{\epsilon^{n+2}}{E_\gamma^{n+2}} - \frac{\epsilon}{E_\gamma} \left(1 + \frac{\epsilon^n}{E_\gamma^n} \right) \right]. \quad (3)$$

In the ultra relativistic limit $E_\gamma \gg m_e$ and $E_\gamma \gg \epsilon$, this equation reduces to

$$\delta_{\gamma,n} E_\gamma^{n+2} + 4E_\gamma \epsilon - m_e^2 \frac{1}{K(1-K)} = 0. \quad (4)$$

Equation 4 implies two scenarios: I) $\delta_{\gamma,n} > 0$ the photo production threshold energy is shifted to lower energies and II) $\delta_{\gamma,n} < 0$ the threshold takes place at higher energies than that expected in a LI regime, except for scenarios below a critical value for delta where the photo production process is forbidden. Figure 1 shows the solution of equation 4 in an innovative way for $n = 0$. The inelasticity is fixed to $K = 1/2$. Three panels are shown: the left panel corresponds to $\delta_{\gamma,0} < 0$, the center panel corresponds to the LI solution with $\delta_{\gamma,0} = 0$ and the right panel to the solution with $\delta_{\gamma,0} > 0$. The gray areas show the allowed regions of E_γ as a function of $\delta_{\gamma,0}$. The boundary of the shaded areas represents the allowed solutions of equation 4 when the background photon energy is equal to 2.7, 2, 1.5, 1 and 0.5 K, from darker to lighter gray, respectively. The allowed regions are cumulative, the allowed area for 1 K includes higher temperatures. The red dashed line is the solution of equation 4 for $\delta_{\gamma,0} = 0$ (LI case) and $T = 2.7$ K. The red dashed line is shown in the left and right panels as a reference. Similar figures were produced for $n = 1, 2$, resulting in the same conclusions. In this work, the effects for $\delta_{\gamma,n} > 0$ are negligible when compared to $\delta_{\gamma,n} < 0$, therefore only the negative case will be discussed in the next sections.

Notice that, if $\delta_{\gamma,n} = 0$ in equation 4 the LI regime is recovered. In the LI regime, it is possible to define $E_\gamma^{LI} = \frac{m_e^2}{4\epsilon K(1-K)}$. The math can be simplified by the introduction of the dimensionless variables

$$x_\gamma = \frac{E_\gamma}{E_\gamma^{LI}}, \quad (5)$$

and

$$\Lambda_{\gamma,n} = \frac{E_\gamma^{LI(n+1)}}{4\epsilon} \delta_{\gamma,n}. \quad (6)$$

Then, equation 4 takes the form

$$\Lambda_{\gamma,n} x_\gamma^{n+2} + x_\gamma - 1 = 0. \quad (7)$$

Studying the values of $\delta_{\gamma,n}$ for which equation 7 has a solution, one can set the extreme allowed LIV coefficient (Galaverni & Sigl (2008b); Martínez-Huerta & Pérez-Lorezana (2017)). The limit LIV coefficient ($\delta_{\gamma,n}^{lim}$) for which the interaction is kinematically allowed for a given E_γ and ϵ is given by:

$$\delta_{\gamma,n}^{lim} = -4 \frac{\epsilon}{E_\gamma^{LI(n+1)}} \frac{(n+1)^{n+1}}{(n+2)^{n+2}}. \quad (8)$$

Figure 1 also shows $\delta_{\gamma,0}^{lim}$ as blue points. Equation 7 has real solutions for x_γ only if $\delta_{\gamma,n} > \delta_{\gamma,n}^{lim}$. Therefore, under the LIV model considered here, if $\delta_{\gamma,n} < \delta_{\gamma,n}^{lim}$, high energy photons would not interact with background photons of energy ϵ .

For a given E_γ and $\delta_{\gamma,n}$ the threshold background photon energy (ϵ_{th}^{LIV}) including LIV effects is:

$$\epsilon_{th}^{LIV} = \frac{m_e^2}{4E_\gamma K(1-K)} - \frac{\delta_{\gamma,n} E_\gamma^{n+1}}{4}. \quad (9)$$

The superscript LIV is used from now on for emphasis. In the next sections, ϵ_{th}^{LIV} as given by equation 9 will be used for the calculations of the mean free path of the $\gamma\gamma_{CB} \rightarrow e^+e^-$ interaction. Figure 2 shows the allowed parameter space of E_γ and ϵ for different values of $\delta_{\gamma,0}$. The gray areas are cumulative from darker to lighter gray.

3. PHOTON HORIZON INCLUDING LIV EFFECTS

The optical depth, $\tau_\gamma(E_\gamma, z)$, quantifies how opaque to photons the Universe is. The survival probability, i.e., the probability that a photon, γ , emitted with a given energy, E_γ , and at a given redshift, z , reaches Earth without interacting with the background, is given by:

$$P_{\gamma \rightarrow \gamma}(E_\gamma, z) = e^{-\tau_\gamma(E_\gamma, z)}. \quad (10)$$

The photon horizon is the distance (z_h) for which $\tau_\gamma(E_\gamma, z_h) = 1$. z_h defines, as a function of the energy of the photon, the redshift at which a emitted photon will have probability $P_{\gamma \rightarrow \gamma} = 1/e$ of reaching Earth. The evaluation of the photon horizon is of extreme importance because it summarizes the visible Universe as a function of the energy of the emitted photon. In this section, the photon horizon is calculated including LIV effects. The argument presented in reference [De Angelis et al. \(2013\)](#) is followed here.

In the intergalactic medium, the $\gamma\gamma_{CB} \rightarrow e^+e^-$ interaction is the main contribution to determine the photon horizon. In the approximation where cosmological effects are negligible, the mean free path, $\lambda(E_\gamma)$, of this interaction is given by:

$$\lambda(E_\gamma) = \frac{cz}{H_0 \tau_\gamma(E_\gamma, z)}, \quad (11)$$

where $H_0 = 70 \text{ km s}^{-1} \text{ Mpc}^{-1}$ is the Hubble constant and c is the speed of light in vacuum. The optical depth is obtained by:

$$\tau_\gamma(E_\gamma, z) = \int_0^z dz \frac{c}{H_0(1+z)\sqrt{\Omega_\Lambda + \Omega_M(1+z)^3}} \times \int_{-1}^1 d(\cos \theta) \frac{1 - \cos \theta}{2} \int_{\epsilon_{th}^{LIV}}^\infty d\epsilon n_\gamma(\epsilon, z) \sigma(E_\gamma, \epsilon, z), \quad (12)$$

where θ is the angle between the direction of propagation of both photons $\theta = [-\pi, +\pi]$, $\Omega_\Lambda = 0.7$ is the dark energy density, $\Omega_M = 0.3$ is the matter density, σ is the cross-section of the interaction and ϵ_{th}^{LIV} is the threshold energy of the interaction as given by equation 9.

$n_{\gamma_{CB}}$ is the background photon density. The dominant backgrounds are the Extra-galactic Background Light (EBL) for $E_\gamma < 10^{14.5} \text{ eV}$, the Cosmic Background Microwave Radiation (CMB) for $10^{14.5} \text{ eV} < E_\gamma < 10^{19} \text{ eV}$ and the Radio Background (RB) for $E_\gamma > 10^{19} \text{ eV}$. In the calculations presented here, the Gilmore model ([Gilmore & Ramirez-Ruiz \(2010\)](#)) was used for the EBL. Since LIV effects in the photon horizon are expected only at the highest energies ($E_\gamma > 10^{16} \text{ eV}$) using different models of EBL would not change the results. For the RB, the data from [Gervasi et al. \(2008\)](#) with a cutoff at 1 MHz were used. Different cutoffs in the RB data lead to different photon horizons as shown in reference [De Angelis et al. \(2013\)](#). Since no new effect shows up in the LIV calculation due to the RB cutoff, only the 1 MHz cutoff will be presented.

It is usual for studies such as the one presented here, in which the threshold of an interaction is shifted causing a modification of the mean free path, to neglect direct effects in the cross section, σ , when solving equation 12. However an implicit change of the cross section is taken into account given its dependence on the energy threshold ϵ_{th}^{LIV} . Thus, the [Breit & Wheeler \(1934\)](#) cross-section was used:

$$\sigma(E, \epsilon, \theta) = \frac{2\pi\alpha^2}{3m_e^2} W(\beta), \quad (13)$$

with

$$W(\beta) = (1 - \beta^2) \times \left[2\beta (\beta^2 - 2) + (3 - \beta^2) \ln \left(\frac{1 + \beta}{1 - \beta} \right) \right], \quad (14)$$

where β refers to the speed of the electron-positron pair in the center-of-mass reference frame:

$$\beta(E, \epsilon, \theta) = \left(1 - \frac{2m_e^2 c^4}{E\epsilon(1 - \cos \theta)} \right)^{1/2}. \quad (15)$$

Figures 3, 4 and 5 show the mean free path for $\gamma\gamma_{CB} \rightarrow e^+e^-$ as a function of the energy of the photon, E_γ , for several LIV coefficients with $n = 0$, $n = 1$ and $n = 2$, respectively. The main effect is an increase in the mean free path that becomes stronger the larger the photon energy, E_γ , and the LIV coefficient are. Consequently, fewer interactions happen and the photon, γ , will have a higher probability of traveling farther than it would have in a LI scenario. Similar effects due to LIV are seen for $n = 0$, $n = 1$ and $n = 2$. The LIV coefficients are treated as free parameters, therefore there is no way to compare the importance of the effect between the orders $n = 0$, $n = 1$ and $n = 2$, each order must be limited independently. Note that $\delta_{\gamma,n}$ units depend on n .

The LIV effect becomes more tangible in figure 6 in which the photon horizon (z_h) is shown as a function of E_γ for $n = 0$. For energies above $E_\gamma > 10^{16.5}$ eV and the given LIV values, the photon horizon increases when LIV is taken into account increasing the probability that a distant source emitting high energy photons produces a detectable flux at Earth. Similar results are found for $n = 1$ and $n = 2$.

4. FLUX OF GZK PHOTONS INCLUDING LIV EFFECTS

Even though the effects of LIV on the propagation of high energy photons are strong, they cannot be directly measured and, therefore, used to probe LIV models. In order to do that, in this section, the flux of GZK photons on Earth considering LIV is obtained and compared to the upper limits on the photon flux from the Pierre Auger Observatory (The Pierre Auger Collaboration (2017a); Carla Bleve for the Pierre Auger Collaboration (2015)).

UHECRs interact with the photon background producing pions (photo-pion production). Pions decay shortly after production generating EeV photons among other particles. The effect of this interaction chain suppresses the primary UHECR flux and generates a secondary flux of photons (Gelmini et al. (2007)). The effect was named GZK after the authors of the original papers (Greisen (1966); Zatsepin & Kuz'min (1966)). The EeV photons (GZK photons) also interact with the background photons as described in the previous sections.

In order to consider LIV in the GZK photon calculation the CRPropa3/Eleca (Batista et al. (2016); Settimo & Domenico (2015)) programs were modified. The mean free paths calculated in section 3 were implemented in the CRPropa3/Eleca codes and the propagation of the particles was simulated. The resulting flux of GZK photons is, however, extremely dependent on the assumptions about the sources of cosmic rays, such as the injected energy spectra, mass composition, and the distribution of sources in the Universe. Therefore, four different models for the injected spectra of cosmic rays at the sources and five different models for the evolution of sources with redshift are considered in the calculations presented below.

4.1. Models of UHECR sources

No source of UHECR was ever identified and correlations studies with types of source are not conclusive. Several source types and mechanisms of particle production have been proposed. The amount of GZK photons produced in the propagation of the particles depends significantly on the source model used. In this paper, four UHECRs source models are used to calculate the corresponding GZK photons. The models are used as illustration of the differences in the production of GZK photons, an analysis of the validity of the models and its compatibility with experimental data is beyond the scope of this paper. However, it is important to note that strong constraints can be set by new measurements (The Pierre Auger Collaboration (2017b)). The models used here are labeled as:

- C_1 : Aloisio, Berezhinsky & Blasi (2014) (Aloisio et al. (2014));
- C_2 : Unger, Farrar & Anchordoqui (2015) - Fiducial model (Unger et al. (2015));
- C_3 : Unger, Farrar & Anchordoqui (2015) (Unger et al. (2015)) with the abundance of galactic nuclei from (Olive & Group (2014));

- **C₄**: Berezhinsky, Gazizov & Grigorieva (2007) - Dip model (Berezhinsky et al. (2006)).

All four models propose the energy spectrum at the source to be a power law distribution on the energy with a rigidity cutoff:

$$\frac{dN}{dE_s} = \begin{cases} E_s^{-\Gamma} & , \text{ for } R_s < R_{cut} \\ E_s^{-\Gamma} e^{1-R_s/R_{cut}} & , \text{ for } R_s \geq R_{cut} \end{cases}, \quad (16)$$

where the spectral index, Γ , and the rigidity cutoff, R_{cut} , are parameters given by each model. Five different species of nuclei (H, He, N, Si and Fe) are considered in these models and their fraction (fH , fHe , fN , fSi and fFe) are given in Table 1.

Model	Γ	$\log_{10}(R_{cut}/V)$	fH	fHe	fN	fSi	fFe
C_1	1	18.699	0.7692	0.1538	0.0461	0.0231	0.00759
C_2	1	18.5	0	0	0	1	0
C_3	1.25	18.5	0.365	0.309	0.121	0.1066	0.098
C_4	2.7	∞	1	0	0	0	0

Table 1. Parameters of the four source models used in this paper. Γ is the spectral index, R_{cut} is the rigidity cutoff and fH , fHe , fN , fSi and fFe are the fractions of each nuclei.

Figure 7 shows the dependence of the GZK photon flux on the source model used. The integral of the GZK photon fluxes for LIV case of $\delta_{\gamma,0} = 10^{-20}$ are shown as a function of energy. The use of different LIV coefficients results in a shift up an down in the integral flux for each source model, having negligible changes in each ratio. The dependence on the model is of several orders of magnitude and should be considered in studies trying to impose limits on LIV coefficients.

4.2. Models of source distribution

Figure 6 shows how the photon horizon increases significantly when LIV is considered. Therefore the source distribution in the Universe is an important input in GZK photon calculations usually neglected in previous studies. Five different models of source evolution(R_n) are considered here:

- **R₁**: Sources are uniformly distributed in a comoving volume;
- **R₂**: Sources follow the star formation distribution given in reference Hopkins & Beacom (2006). The evolution is proportional to $(1+z)^{3.4}$ for $z < 1$, to $(1+z)^{-0.26}$ for $1 \leq z < 4$ and to $(1+z)^{-7.8}$ for $z \geq 4$;
- **R₃**: Sources follow the star formation distribution given in reference Yksel et al. (2008). The evolution is proportional to $(1+z)^{3.4}$ for $z < 1$, to $(1+z)^{-0.3}$ for $1 \leq z < 4$ and to $(1+z)^{-3.5}$ for $z \geq 4$;
- **R₄**: Sources follow the GRB rate evolution from reference Le & Dermer (2007). The evolution is proportional to $(1+8z)/[1+(z/3)^{1.3}]$;
- **R₅**: Sources follow the GRB rate evolution from reference Le & Dermer (2007). The evolution is proportional to $(1+11z)/[1+(z/3)^{0.5}]$.

Figure 8 shows the ratio of sources as a function of redshift for the five source distributions considered. The source evolution uniformly distributed in a comoving volume is shown only for comparison. It is clear that even astrophysical motivated evolution are different for redshift larger than two. Charged particles produced in sources farther than redshift equals to one have a negligible probability of reaching Earth, however the GZK photons produced in their propagation could travel farther if LIV is considered.

Figure 9 shows the effect of the source evolution in the prediction of GZK photons including LIV effects. The use of different LIV coefficients results in a shift up an down in the integral flux for each source evolution model, having negligible changes in each ratio. The differences for each source evolution model are as large as 500% at $E = 10^{18}$ eV.

Model	$\delta_{\gamma,0}^{limit}$	$\delta_{\gamma,1}^{limit} [\text{eV}^{-1}]$	$\delta_{\gamma,2}^{limit} [\text{eV}^{-2}]$
C_1R_5	$\sim -10^{-20}$	$\sim -10^{-38}$	$\sim -10^{-56}$
C_2R_5	-	-	-
C_3R_5	$\sim -10^{-20}$	$\sim -10^{-38}$	$\sim -10^{-56}$
C_4R_5	$\sim -10^{-22}$	$\sim -10^{-42}$	$\sim -10^{-60}$

Table 2. Limits on the LIV coefficients imposed by this work for each source model and LIV order, n .

5. LIMITS ON LIV COEFFICIENTS

The GZK photon flux of the five astrophysical models shown above are considered together with the upper limits on the photon flux imposed by the Pierre Auger Observatory to set limits on the LIV coefficients. The simulations considered sources up to 9500 Mpc ($z \approx 8.88$). Results are shown only for R_5 source evolution, as this is the model for which a stronger flux is produced. The three orders of LIV ($n = 0, 1$ and 2) are considered for each astrophysical model C_i . Two limiting cases are also considered: LI and maximum LIV, labeled as $\delta_\gamma = 0$ and $\delta_\gamma \rightarrow -\infty$, respectively. The Lorentz Invariant case (LI) is shown for comparison. The maximum LIV case ($\delta_\gamma \rightarrow -\infty$) represents the limit in which the mean free path of the photon-photon interaction goes to infinity and therefore no interaction happens at all energies. These two cases bracket the possible LIV solutions. The UHECR flux reaching Earth was normalized to the flux measured by the Pierre Auger Observatory (Inés Valiño for the Pierre Auger Collaboration (2015)) at $E = 10^{18.75}$ eV which sets the normalization of the GZK photon flux produced in the propagation of these particles.

Figures 10-12 show the results of the calculations. Models C_1R_5 , C_3R_5 and C_4R_5 produces more GZK photons than the upper limits imposed by Auger, therefore, upper limits on the LIV coefficients can be imposed. Model C_2R_5 produces less GZK photons than the upper limits imposed by Auger even for the most extreme scenarios therefore no limits on the LIV coefficients could be imposed.

Table 2 shows the limits imposed in this work for each source model and LIV order. Table 3 shows the limits imposed by other works for comparison. The first two references in table 3 are based on energy dependent arrival time of TeV photons, the first one based on the PKS 2155-304 flare measured with H.E.S.S. (The H.E.S.S. Collaboration (2011)) and the second one based on the GRB 090510 measured with Fermi-LAT (Vasileiou et al. (2013)). The last two references in table 3 are based on the kinematics of the interactions of photons with the background photons. One of them uses data from Mrk 501 measured with H.E.S.S. (Lorentz, Matthias & Brun, Pierre (2017)), which is also of the order of TeV. The last one (Galaverni & Sigl (2008a)) uses GZK photons similar to the calculations presented here.

The energy regime studied by gamma-ray experiments (GeV-TeV) and UHECR experiment (EeV) explain the differences of the limits shown in table 3. The differences between the calculations presented here and the limits imposed in reference Galaverni & Sigl (2008a) can be explained by: a) the different assumptions considered in the $\gamma\gamma$ interactions with LIV, b) the different astrophysical models used and c) the upper limit on the GZK photon flux used. In reference Galaverni & Sigl (2008a), the limits were obtained by calculating the energy in which the interaction of a high energy photon with a background photon at the peak of the CMB, i.e., with energy $\epsilon = 6 \times 10^{-4}$ eV, becomes kinematically forbidden. In this work, a more complete approach was used, where the energy threshold was calculated, the mean free path was obtained by integrating the whole background photon spectrum and the propagation was simulated, obtaining the intensity of the flux of GZK photons. The astrophysical scenario used in reference Galaverni & Sigl (2008a) was a pure proton composition with energy spectrum normalized by the AGASA measurement (The AGASA Collaboration (2006)) and index $\Gamma = 2.6$. The source distribution was not specified in the study. However, this astrophysical scenario is ruled out by the X_{max} measurements from the Pierre Auger Observatory (The Pierre Auger Collaboration (2014a,b)). In the calculations presented here, the LIV limits were updated using astrophysical scenarios compatible to the Auger X_{max} data. Finally, in this paper new GZK photons limits published by Auger are used.

6. CONCLUSIONS

In this paper, the effect of possible LIV in the propagation of photons in the Universe is studied. The interaction of a high energy photon traveling in the photon background was solved under LIV in the photon sector hypothesis. An innovative illustration of the solution was presented in section 2.

Model	$\delta_{\gamma,0}^{limit}$	$\delta_{\gamma,1}^{limit} [\text{eV}^{-1}]$	$\delta_{\gamma,2}^{limit} [\text{eV}^{-2}]$
H.E.S.S. - PKS 2155-304 (2011)	-	-4.76×10^{-28}	-2.44×10^{-40}
Fermi - GRB 090510 (2013)	-	-9.62×10^{-29}	-5.92×10^{-41}
H.E.S.S. - Mrk 501 (2017)	-	-1.08×10^{-29}	-4.53×10^{-42}
Galaverni & Sigl (2008)	-	-1.97×10^{-43}	-1.61×10^{-63}

Table 3. Limits on the LIV coefficients imposed by other works in astrophysics.

The mean free path of the $\gamma\gamma_{CB} \rightarrow e^+e^-$ interaction was calculated considering LIV effects. Moderate LIV coefficients introduce a significant change in the mean free path of the interaction as shown in section 3 and figures 3, 4 and 5. The corresponding LIV photon horizon was calculated as shown in figure 6.

The dependence of integral flux of GZK photon on the model for the sources of UHECRs is discussed in section 4 and shown in figures 7 and 9. The flux changes several orders of magnitude for different injection spectra models. A difference of about 500% is also found for different source evolution models. The fluxes were compared to the upper limits from the Pierre Auger Observatory and are shown in figures 10-12. For some of the models, it was possible to impose limits on the LIV coefficients, as shown in table 2. These limits are several orders of magnitude more restrictive than those found using TeV photons and more conservative and up to date than the previous ones for GZK photons.

RGL is supported by FAPESP (2014/26816-0, 2016/24943-0). HMH acknowledges IFSC/USP for their hospitality during the developments of this work, Abdel Pérez Lorenzana for enlightening discussions and the support from Conacyt Mexico under grant 237004 and the Brazilian agency FAPESP (2017/03680-3). VdS thanks the Brazilian population support via FAPESP (2015/15897-1) and CNPq. This work has partially made use of the computing facilities of the Laboratory of Astroinformatics (IAG/USP, NAT/Unicsul), whose purchase was made possible by the Brazilian agency FAPESP (2009/54006-4) and the INCT-A. The authors acknowledge the National Laboratory for Scientific Computing (LNCC/MCTI, Brazil) for providing HPC resources of the SDumont supercomputer, which have contributed to the research results reported within this paper (<http://sdumont.lncc.br>).

REFERENCES

- Aloisio, R., Berezhinsky, V., & Blasi, P. 2014, *Journal of Cosmology and Astroparticle Physics*, 2014, 020.
<http://stacks.iop.org/1475-7516/2014/i=10/a=020>
- Amelino-Camelia, G., Ellis, J. R., Mavromatos, N. E., Nanopoulos, D. V., & Sarkar, S. 1998, *Nature*, 393, 763
- Atwood, W. B., et al. 2009, *The Astrophysical Journal*, 697, 1071.
<http://stacks.iop.org/0004-637X/697/i=2/a=1071>
- Batista, R. A., Dundovic, A., Erdmann, M., et al. 2016, *Journal of Cosmology and Astroparticle Physics*, 2016, 038.
<http://stacks.iop.org/1475-7516/2016/i=05/a=038>
- Berezhinsky, V., Gazizov, A., & Grigorieva, S. 2006, *Phys. Rev. D*, 74, 043005. <https://link.aps.org/doi/10.1103/PhysRevD.74.043005>
- Breit, G., & Wheeler, J. A. 1934, *Phys. Rev.*, 46, 1087.
<http://link.aps.org/doi/10.1103/PhysRev.46.1087>
- Carla Bleve for the Pierre Auger Collaboration. 2015, *Proceedings of Science (ICRC2015)*, 1103.
<https://pos.sissa.it/236/1103/pdf>
- Coleman, S., & Glashow, S. L. 1999, *Phys. Rev. D*, 59, 116008
- De Angelis, A., Galanti, G., & Roncadelli, M. 2013, *Monthly Notices of the Royal Astronomical Society*, doi:10.1093/mnras/stt684.
<http://mnras.oxfordjournals.org/content/early/2013/05/21/mnras.stt684.abstract>
- Galaverni, M., & Sigl, G. 2008a, *Phys. Rev. Lett.*, 100, 021102
- . 2008b, *Phys. Rev.*, D78, 063003
- Gelmini, G., Kalashev, O., & Semikoz, D. V. 2007, *Astroparticle Physics*, 28, 390 .
<http://www.sciencedirect.com/science/article/pii/S0927650507001004>
- Gervasi, M., Tartari, A., Zannoni, M., Boella, G., & Sironi, G. 2008, *The Astrophysical Journal*, 682, 223.
<http://stacks.iop.org/0004-637X/682/i=1/a=223>
- Gilmore, R., & Ramirez-Ruiz, E. 2010, *The Astrophysical Journal*, 721, 709.
<http://stacks.iop.org/0004-637X/721/i=1/a=709>

- Greisen, K. 1966, Phys. Rev. Lett., 16, 748.
<http://link.aps.org/abstract/PRL/v16/p748>
- Haungs, A., Medina-Tanco, G., & Santangelo, A. 2015, Experimental Astronomy, 40, 1.
<http://dx.doi.org/10.1007/s10686-015-9483-9>
- Hopkins, A. M., & Beacom, J. F. 2006, The Astrophysical Journal, 651, 142.
<http://stacks.iop.org/0004-637X/651/i=1/a=142>
- Inés Valiño for the Pierre Auger Collaboration. 2015, Proceedings of Science (ICRC2015), 271.
https://pos.sissa.it/archive/conferences/236/271/ICRC2015_271.pdf
- Jacobson, T., Liberati, S., & Mattingly, D. 2003, Phys. Rev., D67, 124011
- Klinkhamer, F. R., & Schreck, M. 2008, Phys. Rev., D78, 085026
- Le, T., & Dermer, C. D. 2007, The Astrophysical Journal, 661, 394.
<http://stacks.iop.org/0004-637X/661/i=1/a=394>
- Liberati, S., & Maccione, L. 2009, Annual Review of Nuclear and Particle Science, 59, 245.
<http://www.annualreviews.org/doi/abs/10.1146/annurev.nucl.010909.083640>
- . 2011, J. Phys. Conf. Ser., 314, 012007
- Lorentz, Matthias, & Brun, Pierre. 2017, EPJ Web Conf., 136, 03018.
<https://doi.org/10.1051/epjconf/201713603018>
- Maccione, L., & Liberati, S. 2008, Journal of Cosmology and Astroparticle Physics, 0808, 027
- Martínez-Huerta, H., & Pérez-Lorenzana, A. 2017, Phys. Rev., D95, 063001
- Mattingly, D. 2005, Living Reviews in Relativity, 8, doi:10.12942/lrr-2005-5.
<http://www.livingreviews.org/lrr-2005-5>
- Benjamin Zitzer for the VERITAS Collaboration. 2014, Braz.J.Phys., 44, 4
- J. Holder for the VERITAS Collaboration. 2011, Proc. International Cosmic Ray Conference, 12
- The AGASA Collaboration. 2006, Nucl.Phys.Proc.Suppl., 3
- The CTA Consortium. 2011, Experimental Astronomy, 32, 193. <http://dx.doi.org/10.1007/s10686-011-9247-0>
- The H.E.S.S. Collaboration. 2006, Astronomy and Astrophysics, 457, 899.
<http://dx.doi.org/10.1051/0004-6361:20065351>
- . 2011, Astropart. Phys., 34, 738
- The MAGIC Collaboration. 2016, Astroparticle Physics, 72, 61. <http://www.sciencedirect.com/science/article/pii/S0927650515000663>
- The Pierre Auger Collaboration. 2014a, Phys. Rev., D90, 122005
- . 2014b, Phys. Rev., D90, 122006
- . 2015, Nuclear Instruments and Methods in Physics Research Section A: Accelerators, Spectrometers, Detectors and Associated Equipment, 798, 172. <http://www.sciencedirect.com/science/article/pii/S0168900215008086>
- . 2017a, Journal of Cosmology and Astroparticle Physics, 2017, 009.
<http://stacks.iop.org/1475-7516/2017/i=04/a=009>
- . 2017b, Journal of Cosmology and Astroparticle Physics, 2017, 038.
<http://stacks.iop.org/1475-7516/2017/i=04/a=038>
- Myers, R. C., & Pospelov, M. 2003, Phys. Rev. Lett., 90, 211601
- Olive, K., & Group, P. D. 2014, Chinese Physics C, 38, 090001.
<http://stacks.iop.org/1674-1137/38/i=9/a=090001>
- Settimo, M., & Domenico, M. D. 2015, Astroparticle Physics, 62, 92. <http://www.sciencedirect.com/science/article/pii/S0927650514001145>
- Stecker, F. W., & Scully, S. T. 2005, Astropart. Phys., 23, 203
- . 2009, New J. Phys., 11, 085003
- Tinyakov, P. 2014, Nuclear Instruments and Methods in Physics Research Section A: Accelerators, Spectrometers, Detectors and Associated Equipment, 742, 29, 4th Roma International Conference on Astroparticle Physics.
<http://www.sciencedirect.com/science/article/pii/S0168900213014587>
- Unger, M., Farrar, G. R., & Anchordoqui, L. A. 2015, Phys. Rev. D, 92, 123001. <https://link.aps.org/doi/10.1103/PhysRevD.92.123001>
- Vasileiou, V., Jacholkowska, A., Piron, F., et al. 2013, Phys. Rev. D, 87, 122001. <https://link.aps.org/doi/10.1103/PhysRevD.87.122001>
- Yksel, H., Kistler, M. D., Beacom, J. F., & Hopkins, A. M. 2008, The Astrophysical Journal Letters, 683, L5.
<http://stacks.iop.org/1538-4357/683/i=1/a=L5>
- Zatsepin, G. T., & Kuz'min, V. A. 1966, ZhETF Pis'ma, 4, 114

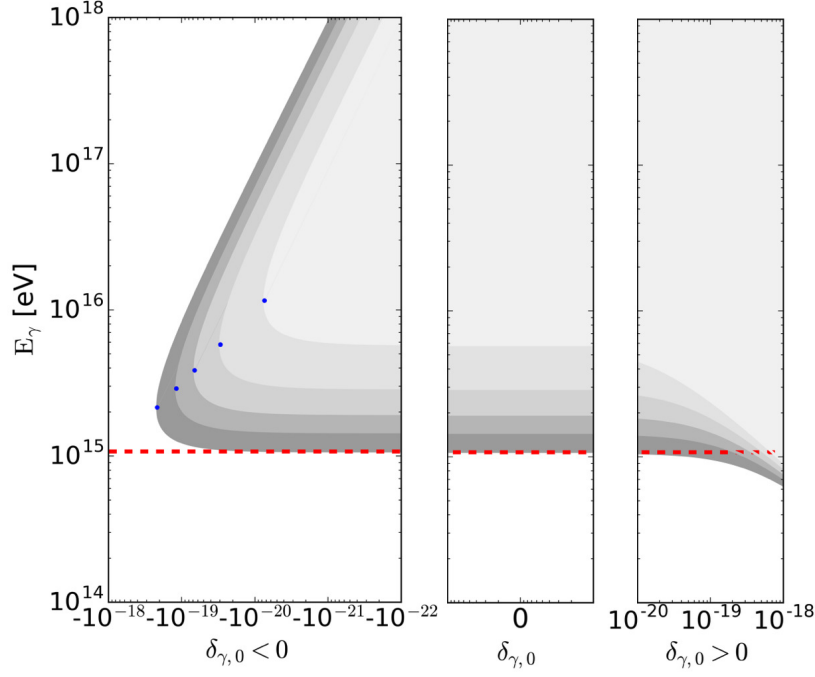


Figure 1. Allowed regions of the high energy photon (E_γ) and $\delta_{\gamma,0}$ for the $\gamma\gamma_{CB} \rightarrow e^+e^-$ interaction considering LIV effects. Gray regions show for each case the space parameter for which equation 4 is solvable. The left panel corresponds to $\delta_{\gamma,0} < 0$, the center panel corresponds to the LI solution with $\delta_{\gamma,0} = 0$ and the right panel to the solutions with $\delta_{\gamma,0} > 0$. Five cases of the background photon energy (ϵ) are shown corresponding to temperatures of 2.7, 2, 1.5, 1 and 0.5 K, from dark to light gray, respectively. The red dashed line is a reference for $\delta_{\gamma,0} = 0$ (LI case) with ϵ corresponding to 2.7 K. The blue points represents $\delta_{\gamma,0}^{lim}$ as calculated in equation 8.

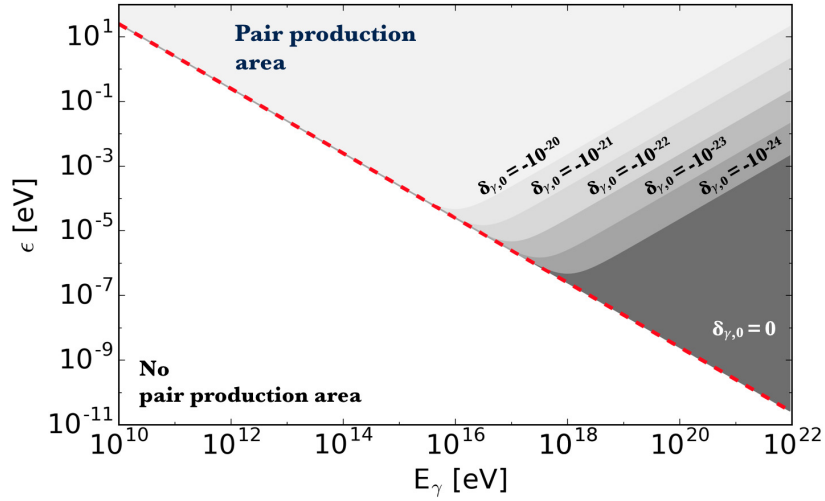


Figure 2. Allowed regions for the pair production in the $\gamma\gamma_{CB} \rightarrow e^+e^-$ interaction considering LIV effects. The high energy photon (E_γ) and background photon (ϵ) parameter space is shown divided in gray regions for each value of $\delta_{\gamma,0}$. The gray areas are cumulative from darker to lighter gray. The red dashed line is a reference for $\delta_{\gamma,0} = 0$ (LI case).

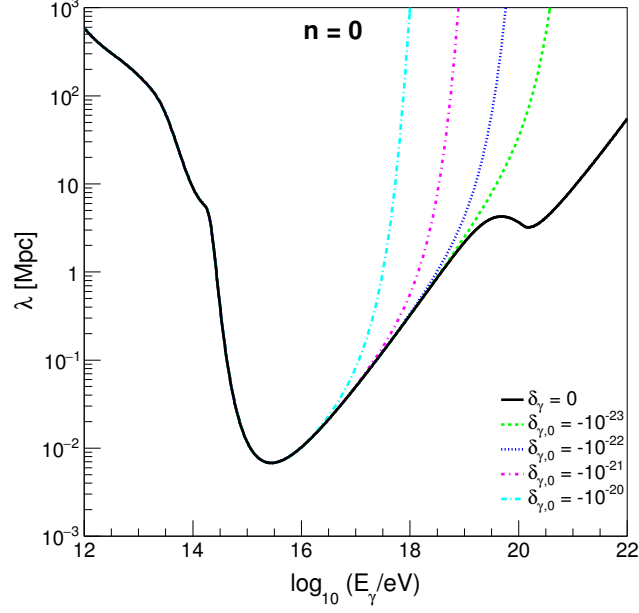


Figure 3. Mean free path (λ) for $\gamma\gamma_{CB} \rightarrow e^+e^-$ as a function of the energy of the photon (E_γ) shown for several LIV coefficients for $n = 0$. The Gilmore model (Gilmore & Ramirez-Ruiz (2010)) for EBL and Gervasi et al. (Gervasi et al. (2008)) model for the RB with a cutoff at 1 MHz were used. The black continuous line is the LI scenario. The colored lines represent different values for the LIV coefficients. The colored lines coincide with the black line for $\log(E_\gamma/\text{eV}) < 15$.

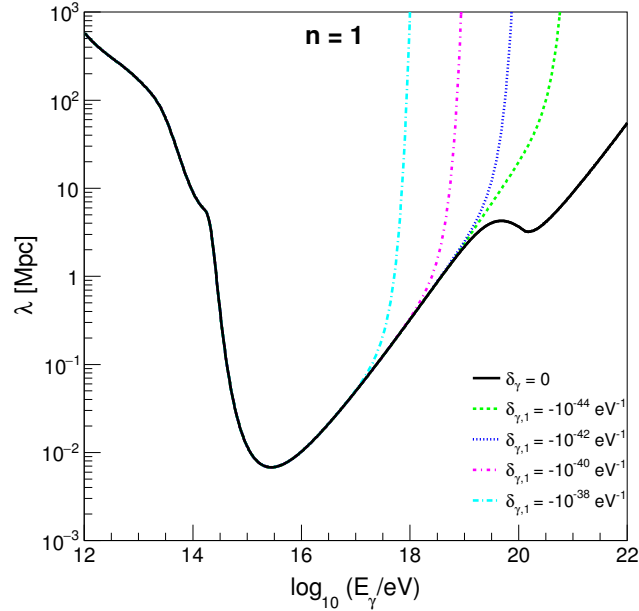


Figure 4. Mean free path (λ) for $\gamma\gamma_{CB} \rightarrow e^+e^-$ as a function of the energy of the photon (E_γ) shown for several LIV coefficients for $n = 1$. The Gilmore model (Gilmore & Ramirez-Ruiz (2010)) for EBL and Gervasi et al. (Gervasi et al. (2008)) model for the RB with a cutoff at 1 MHz were used. The black continuous line is the LI scenario. The colored lines represent different values for the LIV coefficients. The colored lines coincide with the black line for $\log(E_\gamma/\text{eV}) < 15$.

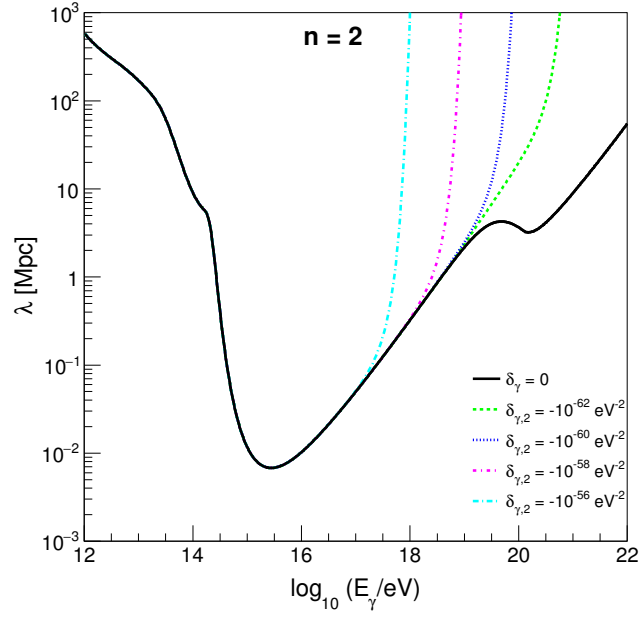


Figure 5. Mean free path (λ) for $\gamma\gamma_{CB} \rightarrow e^+e^-$ as a function of the energy of the photon (E_γ) shown for several LIV coefficients for $n = 2$. The Gilmore model (Gilmore & Ramirez-Ruiz (2010)) for EBL and Gervasi et al. (Gervasi et al. (2008)) model for the RB with a cutoff at 1 MHz were used. The black continuous line is the LI scenario. The colored lines represent different values for the LIV coefficients. The colored lines coincide with the black line for $\log(E_\gamma/\text{eV}) < 15$.

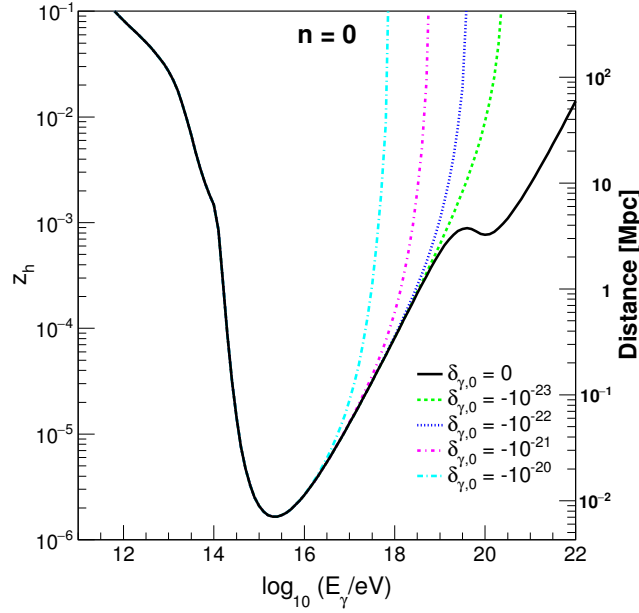


Figure 6. Photon horizon (z_h) as a function of the photon energy (E_γ) for different LIV coefficients with $n = 0$. The right axis shows the equivalent distance obtained using the same assumptions used in equation 12. The Gilmore model (Gilmore & Ramirez-Ruiz (2010)) for EBL and Gervasi et al. (Gervasi et al. (2008)) model for the RB with a cutoff at 1 MHz were used. The black continuous line represents the LI scenario. The colored lines represent different values for the LIV coefficients. The colored lines coincide with the black line for $\log(E_\gamma/\text{eV}) < 15$.

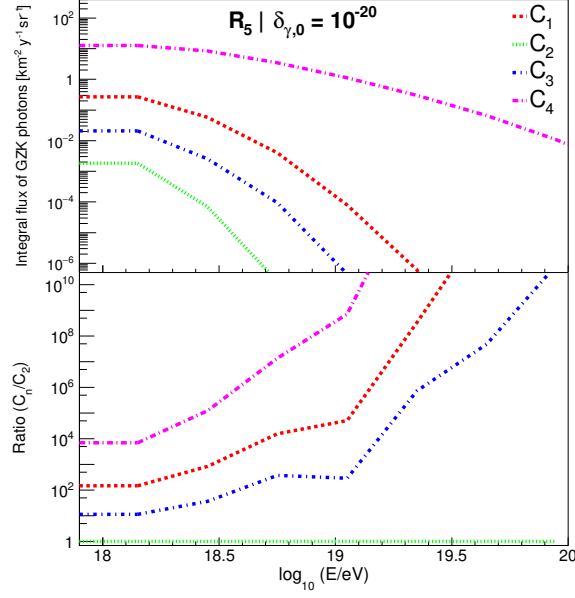


Figure 7. Integral flux of GZK photons as a function of the photon energy for each source model. Each line represents a different model C_n . All cases are for the source evolution model R_5 and LIV coefficient $\delta_{\gamma,0} = 10^{-20}$. The top panel shows the integral flux, while the bottom panel show the ratio to the one that produces less photons, C_2 .

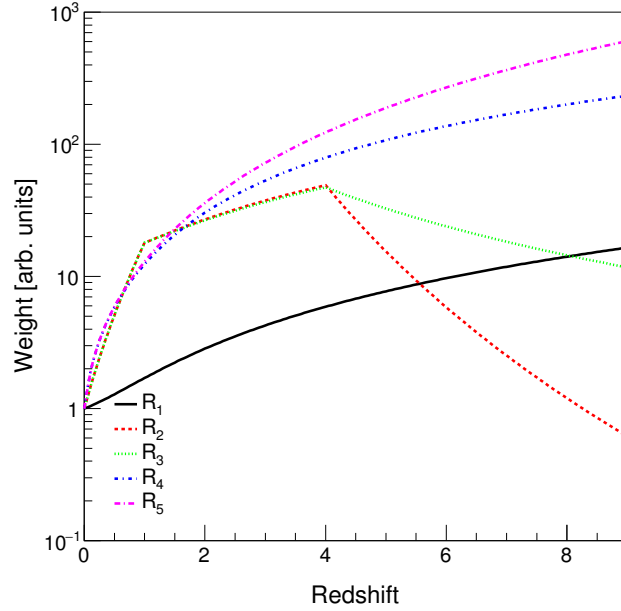


Figure 8. Source evolution with redshift. Each line represents one of the models R_n , see text for details of the models.

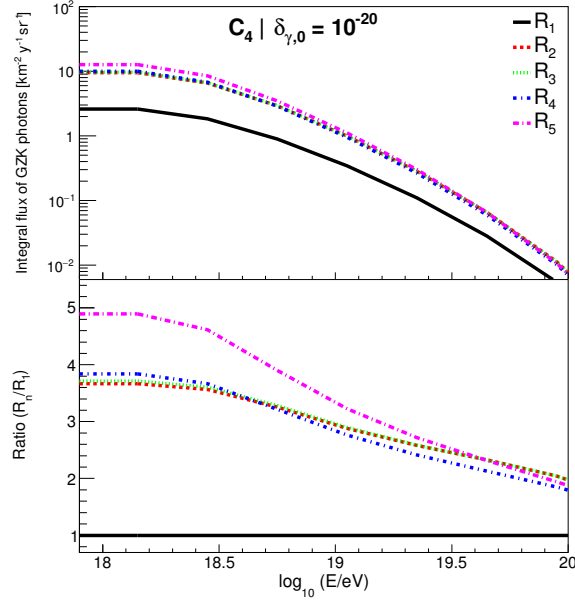


Figure 9. Integral flux of GZK photons as a function of the photon energy for each source evolution model. Each line represents a different model R_n . All cases are for the source model C_4 and LIV coefficient $\delta_{\gamma,0} = 10^{-20}$. The top panel shows the integral flux, while the bottom panel show the ratio to the simplest case, R_1 .

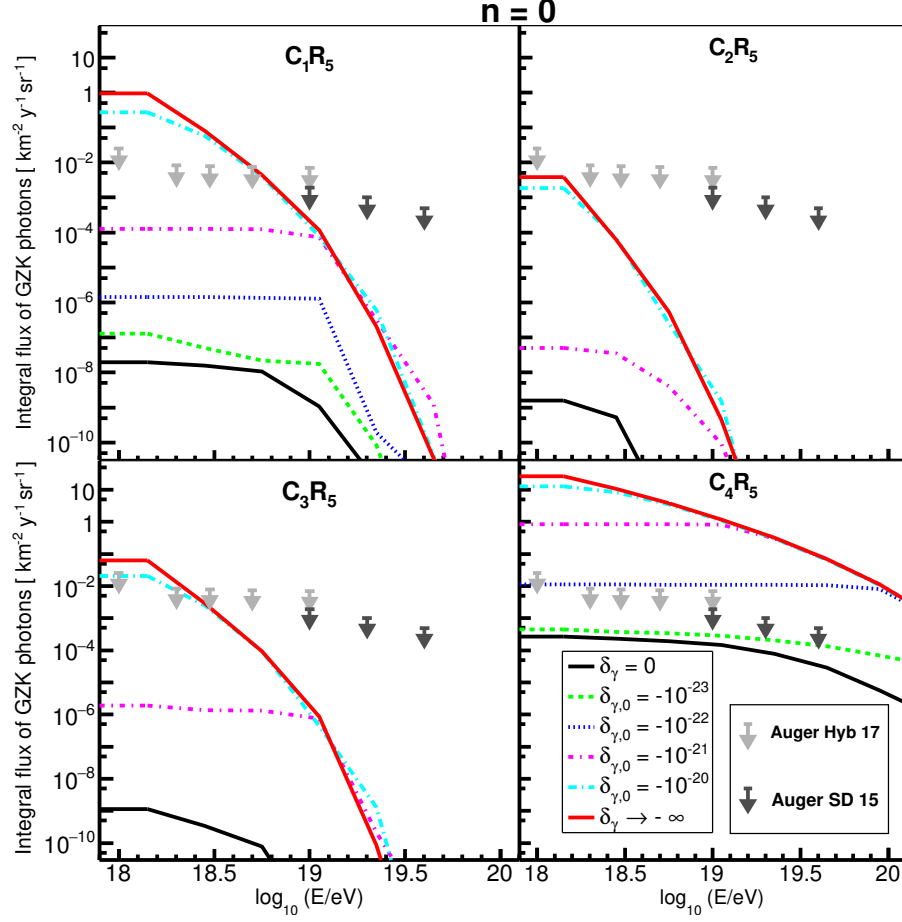


Figure 10. Integral flux of GZK photons as a function of the photon energy considering LIV effects for $n = 0$. The black continuous line represents the LI scenario. The colored lines represent different values for the LIV coefficients. The red line represents the limit LIV case. The arrows represent the upper limits from the Pierre Auger Observatory. Each panel represent a source model, $C_1 R_5$, $C_2 R_5$, $C_3 R_5$, $C_4 R_5$, respectively.

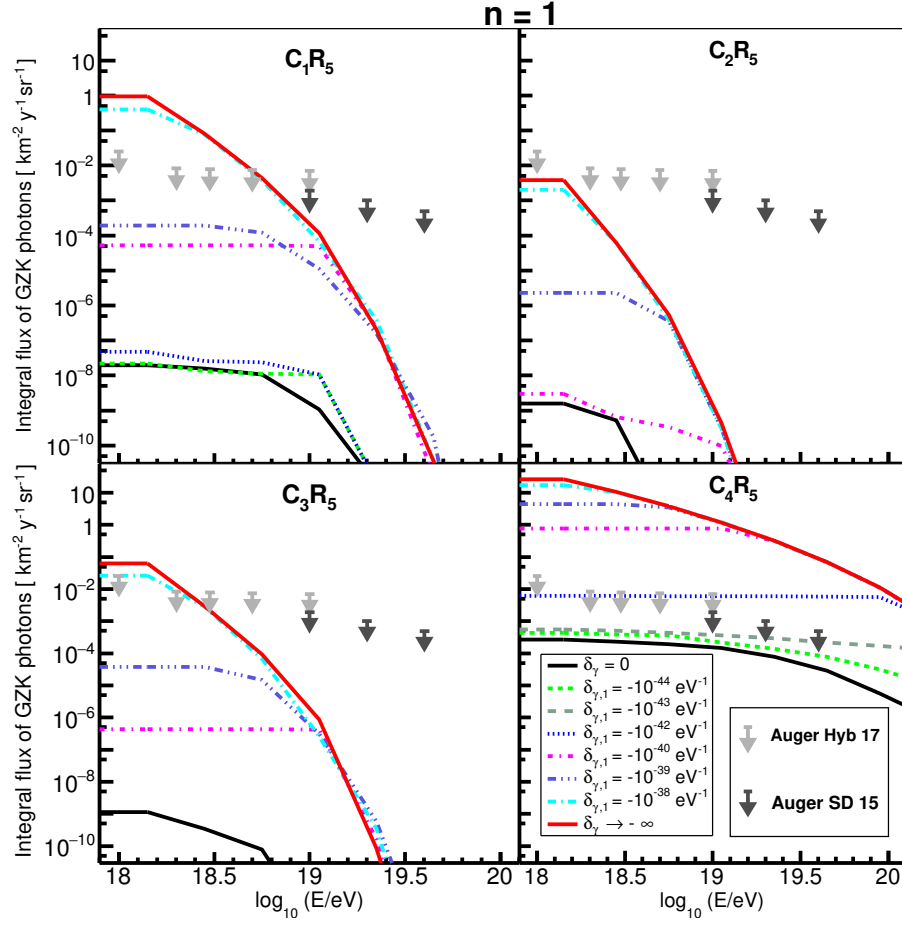


Figure 11. Integral flux of GZK photons as a function of the photon energy considering LIV effects for $n = 1$. The black continuous line represents the LI scenario. The colored lines represent different values for the LIV coefficients. The red line represents the limit LIV case. The arrows represent the upper limits from the Pierre Auger Observatory. Each panel represent a source model, C_1R_5 , C_2R_5 , C_3R_5 , C_4R_5 , respectively.

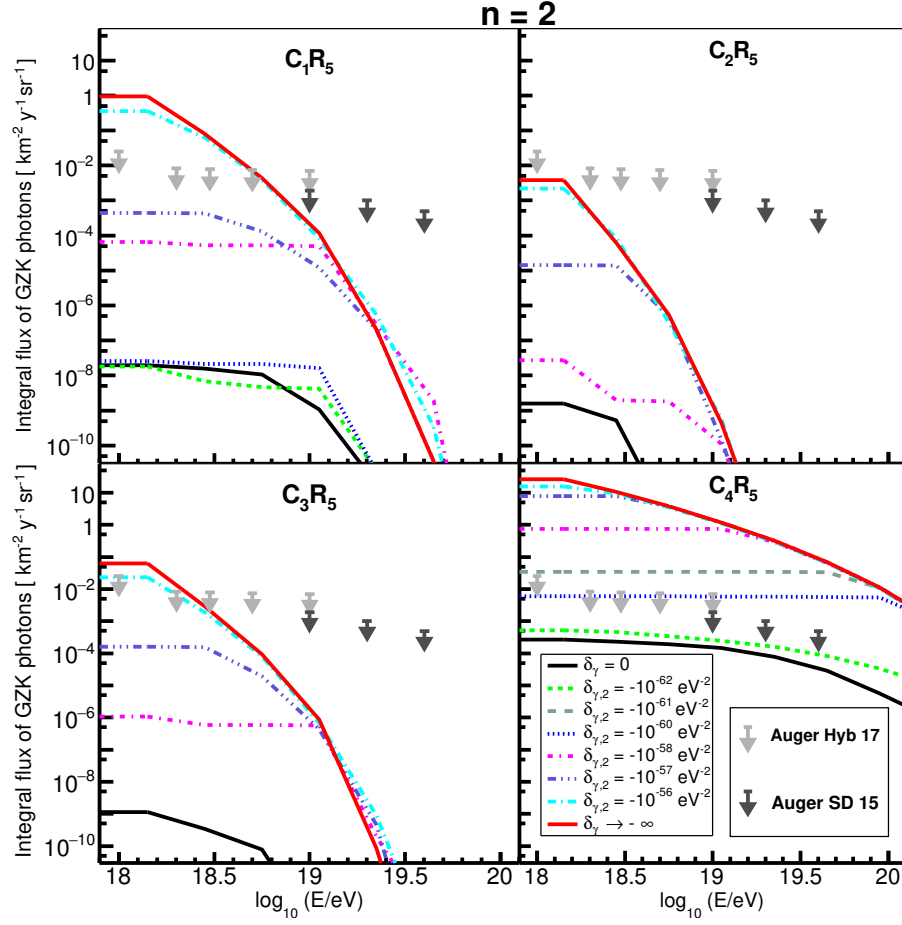


Figure 12. Integral flux of GZK photons as a function of the photon energy considering LIV effects for $n = 2$. The black continuous line represents the LI scenario. The colored lines represent different values for the LIV coefficients. The red line represents the limit LIV case. The arrows represent the upper limits from the Pierre Auger Observatory. Each panel represent a source model, C_1R_5 , C_2R_5 , C_3R_5 , C_4R_5 , respectively.